

Supporting Information for

A Series of Metal-Organic Frameworks for Selective CO₂ Capture and Catalytic Oxidative Carboxylation of Olefins

Huong T. D. Nguyen,^{†,‡} Y B. N. Tran,[‡] Hung N. Nguyen,[‡] Tranh C. Nguyen,[†] Felipe Gándara,^{#,*} and Phuong T. K. Nguyen^{†,‡,*}

[†]Faculty of Chemistry, University of Science, Vietnam National University – Ho Chi Minh City, Ho Chi Minh City 721337, Vietnam

[‡]Center for Innovative Materials and Architectures (INOMAR), Vietnam National University – Ho Chi Minh City, Ho Chi Minh City 721337, Vietnam

[#]Departamento de Nuevas Arquitecturas en Química de Materiales – Materials Science Factory, Instituto de Ciencia de Materiales de Madrid (ICMM-CSIC), Sor Juana Inés de la Cruz 3, Cantoblanco 28049, Madrid, Spain

*To whom correspondence should be addressed: Email, gandara@icmm.csic.es;
ntkphuong@inomar.edu.vn.

Table of Contents

Section S1	Materials and Analytical Techniques	S3 – S4
Section S2	Synthesis of Tetratopic, H ₄ BIPA-TC, Organic Linker	S5
Section S3	Single Crystal X-ray Diffraction Analyses and Optical Images	S6 – S8
Section S4	Topological Analysis	S9 – S10
Section S5	Characterization of MOF-590, -591, and -592	S11 – S16
Section S6	Gas Adsorption Measurements and Selectivity Calculations	S17 – S21
Section S7	Gas Breakthrough Measurement	S22
Section S8	Characterization of Materials for Catalysis	S23 – S27
Section S9	General Procedure and Studies for the One-pot Oxidative Carboxylation of Styrene and CO ₂	S28 – S32
Section S10	Post-Catalysis Characterization of MOF-590.	S33 – S34
Section S11	Mechanism Study for One-pot Oxidative Carboxylation of Styrene and CO ₂	S35 – S36
Section S12	References	S37

Section S1: Materials and Analytical Techniques

Chemical used in this work.

Europium (III) nitrate pentahydrate ($\text{Eu}(\text{NO}_3)_3 \cdot 5\text{H}_2\text{O}$, 99.9%), neodymium (III) nitrate hexahydrate ($\text{Nd}(\text{NO}_3)_3 \cdot 6\text{H}_2\text{O}$, 99.9%), 1,4,5,8-naphthalenetetracarboxylic dianhydride (NTCDA), glacial acetic acid ($\geq 99.85\%$), anhydrous *tert*-butyl hydroperoxide (TBHP, 5.0 – 6.0 M in decane), 2,5-dihydroxyterephthalic acid (H_2DOT , 98%), 2,2'-bipyridine-5,5'-dicarboxylic acid (H_2bpydc , 97%), terephthalic acid (H_2BDC , 98%), 2,2,6,6-tetramethylpiperidine 1-oxyl (TEMPO, 98%), and balloon (wall thickness 1 mil) were obtained from Sigma-Aldrich. 5-aminoisophthalic acid ($\geq 98\%$), *N,N*-dimethylformamide (DMF, 99.8%), anhydrous ethanol (EtOH, 99.5%), styrene (99.5%), tetrabutylammonium bromide ($n\text{Bu}_4\text{NBr}$, 99+%), and aqueous *tert*-butyl hydroperoxide (TBHP, 70% solution in water) were purchased from Acros Organics. Terbium (III) nitrate hydrate ($\text{Tb}(\text{NO}_3)_3 \cdot x\text{H}_2\text{O}$, 99.9%) was purchased from Alfa Aesar. *N,N*-dimethylacetamide (DMAc, $\geq 99.0\%$), ethyl acetate (EtOAc, $\geq 99.5\%$), diethyl ether (Et_2O , $\geq 99.7\%$), and anhydrous sodium sulfate ($\geq 99\%$) was obtained from Merck Chemical Co. Deionized water (ultrapure, 17.8 $\text{M}\Omega \cdot \text{cm}$ resistivity, obtained from a Barnstead Easypure II system). Deuterated solvents, CDCl_3 and $\text{DMSO}-d_6$, were purchased from Cambridge Isotope Laboratories (Andover, MA) and used without further purification. All chemicals were used without further purification unless otherwise noted.

MOF-177 (Basolite Z377), ZIF-8 (Basolite Z1200), MIL-53(Al) (Basolite A100), and HKUST-1 (Basolite C300) were purchased from Sigma-Aldrich. To yield guest-free material, MOF-177, and ZIF-8 were activated under vacuum (10^{-3} Torr) and heated at 120°C for 24 h. MIL-53(Al) was immersed in anhydrous methanol (5 mL) for 1 day before activated under vacuum at ambient temperature for 12 h, followed by heating at 100°C under vacuum for an additional 24 h. The synthesis and activation of Mg-MOF-74 and UiO-67-bpydc was carried out according to a previously reported procedure.^{S1,S2} To assess their structures and porosities, powder X-ray diffraction and N_2 adsorption measurements at 77 K were performed.

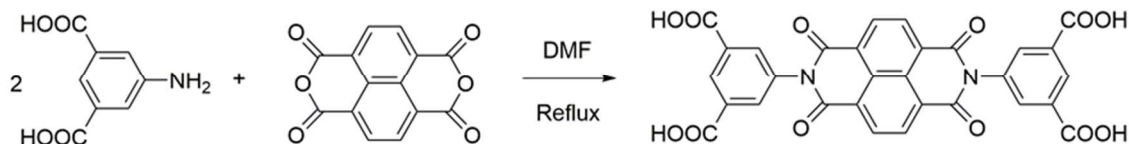
Synthesis of Nd-BDC, $\text{Nd}_2(\text{BDC})_3(\text{DMF})_3 \cdot \text{H}_2\text{O}$. The synthesis of Nd-BDC was carried out, with slight modifications, according to a previously reported procedure.^{S2} A mixture solution of 2.5 mL DMF, 0.50 mL EtOH, and 0.50 mL H_2O were inserted to an 8 mL vial, which was preloaded

with 4.0 mg H₂BDC and 10.9 mg Nd(NO₃)₃·6H₂O. The mixture reaction was sonicated and heated at 85 °C for 48 h, yielding violet crystalline powder. The mother liquor was then decanted, and the solid was washed with DMF (3 × 5 mL) per day for 3 days, then immersed in anhydrous ethanol (3 × 5 mL) per day for 3 days total. The solvent-exchanged sample was activated under vacuum at 50 °C for 24 h. Structure and porosity were confirmed by powder X-ray diffraction and N₂ adsorption measurement at 77 K.

Analytical techniques.

Single crystal X-ray diffraction (SXRD) data for MOF-590 and MOF-592 were obtained in Bruker four circle kappa-diffractometer equipped with a Cu INCOATED microsource, operated at 30 W power (45kV, 0.60mA) to generate Cu K α radiation ($\lambda = 1.54178 \text{ \AA}$), and a Bruker VANTEC 500 area detector (microgap technology). Data for MOF-591 were collected using Bruker D8 Venture diffractometer using monochromatic fine focus Cu K α radiation ($\lambda = 1.54178 \text{ \AA}$). Powder X-ray diffraction (PXRD) data were collected using a Bruker D8 Advance employing Ni-filtered Cu K α ($\lambda = 1.54178 \text{ \AA}$). The system was also outfitted with an anti-scattering shield that prevents incident diffuse radiation from hitting the detector. Samples were placed on zero background sample holders by dropping powders from a spatula and then leveling the sample with a spatula. The 2θ range was 3-50° with a step size of 0.02° and a fixed counting time of 1 s per step. Fourier transform infrared (FT-IR) spectra were measured using KBr pellets on a Bruker Vertex 70 system, and the output signals are described as follows: vs, very strong; s, strong; m, medium; sh, shoulder; w, weak; vw, very weak; br, broad. Optical microscope images were collected on Nikon SMZ1000 Zoom Stereomicroscope. Electrospray-ionization mass spectrometry (ESI-MS) was conducted in negative ionization mode on an Agilent 1200 Series high-performance liquid chromatography coupled to a Bruker micrOTOF-QII mass spectrometer detector. Field-emission Scanning Electron Microscope (FE-SEM) was performed on an ultralow voltage imaging with Hitachi's S-4800 FE-SEM operating at an accelerating voltage of 1 kV.

Section S2: Synthesis of Tetratopic, H₄BIPA-TC, Organic Linker



Scheme S1. Synthetic route to benzoimidephenanthroline tetracarboxylic acid (H₄BIPA-TC).

Benzoimidephenanthroline tetracarboxylic acid (H₄BIPA-TC): H₄BIPA-TC was prepared, with slight modifications, according to a previously reported procedure (Scheme S1).^{S3} A dry 100mL flask was charged with 5-aminoisophthalic acid (3.639 g, 20 mmol) and 1,4,5,8-naphthalenetetracarboxylic acid dianhydride (2.696 g, 10 mmol). DMF (20 mL) were then added to the mixture and the solution was stirred rapidly and refluxed for 8h. The reaction was then allowed to cool to room temperature and filtered over a Buchner funnel. A resulting brown crude solid was washed thoroughly with a mixture of DMF: H₂O (1:1 v/v, 3 × 5 mL), EtOH (2 × 5 mL) and dried at 100 °C overnight to give yellow compound (84 %, 5.02 g). ¹H NMR (300 MHz, DMSO): δ 8.32 (d, *J* = 1.5 Hz, 4H), 8.57 (t, *J* = 1.5 Hz, 2H), 8.72 (s, 4H), 13.46 (br., 4H) ppm. ¹³C NMR (125 MHz, CDCl₃) δ 166.7, 163.5, 136.8, 134.6, 133.2, 130.8, 130.4, 127.7, 127.3 ppm. FT-IR (KBr, pellet, cm⁻¹): 3430 (s, br), 1710 (s), 1677 (s), 1580 (m), 1449 (w), 1351 (s), 1251 (s), 1123 (s), 769 (m), 740 (m), 647 (w). ESI-MS ([M-H]⁻): *m/z* = 593.0485 (found), 593.0463 (calcd. for C₃₀H₁₃O₁₂N₂).

Section S3: Single Crystal X-ray Diffraction (SXRD) Analyses and Optical Images

SXRD Data Collection and Structural Solution of MOF-590

The single crystal data for a yellow needle crystal ($0.12 \times 0.09 \times 0.05 \text{ mm}^3$) was collected at 100 K on a Bruker four circle kappa-diffractometer equipped with a Cu INCOATED microsource, operated at 30 W power (45kV, 0.60mA) to generate Cu $K\alpha$ radiation ($\lambda = 1.54178 \text{ \AA}$), and a Bruker VANTEC 500 area detector (microgap technology).

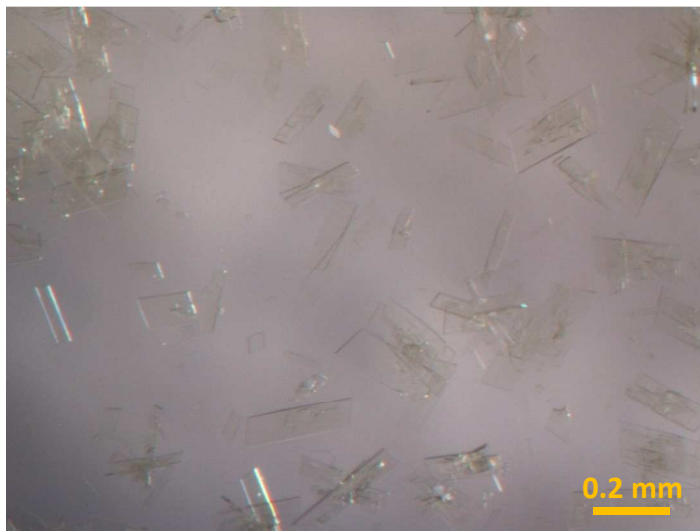


Figure S1. Optical microscope image of MOF-590 showing homogenous crystal morphology.

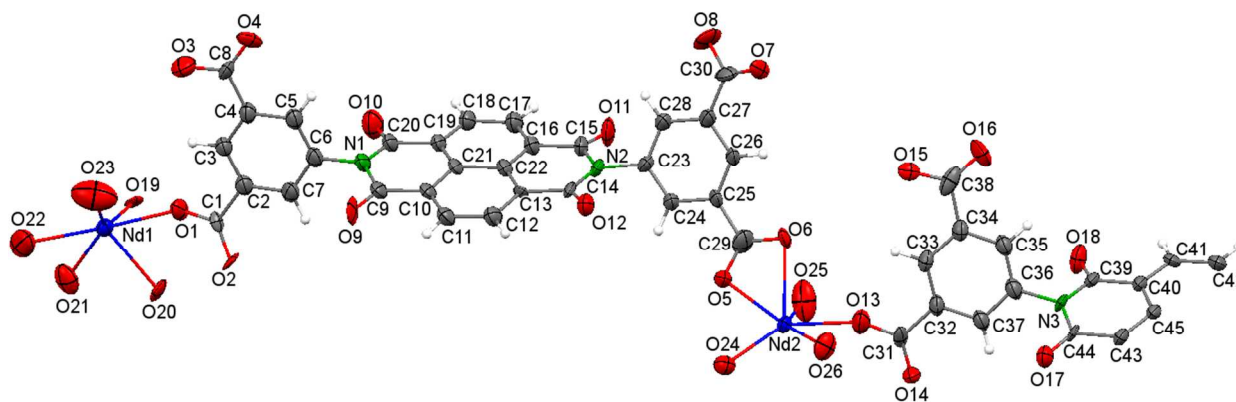


Figure S2. ORTEP representation of the asymmetric unit of MOF-590 displayed with 75% probability. Atom colors: Nd, blue; N, green; O, red; H, white; and C, grey.

SXRD Data Collection and Structural Solution of MOF-592

A yellow block-shaped ($0.2 \times 0.05 \times 0.03 \text{ mm}^3$) crystal of as-synthesized MOF-592 was picked up from the mother liquor and measured at Bruker four circle kappa-diffractometer equipped with a Cu INCOATED microsource, operated at 30 W power (45kV, 0.60mA) to generate Cu $K\alpha$ radiation ($\lambda = 1.54178 \text{ \AA}$), and a Bruker VANTEC 500



area detector (microgap technology).

Figure S5. Optical microscope image of MOF-592 showing homogenous crystal morphology.

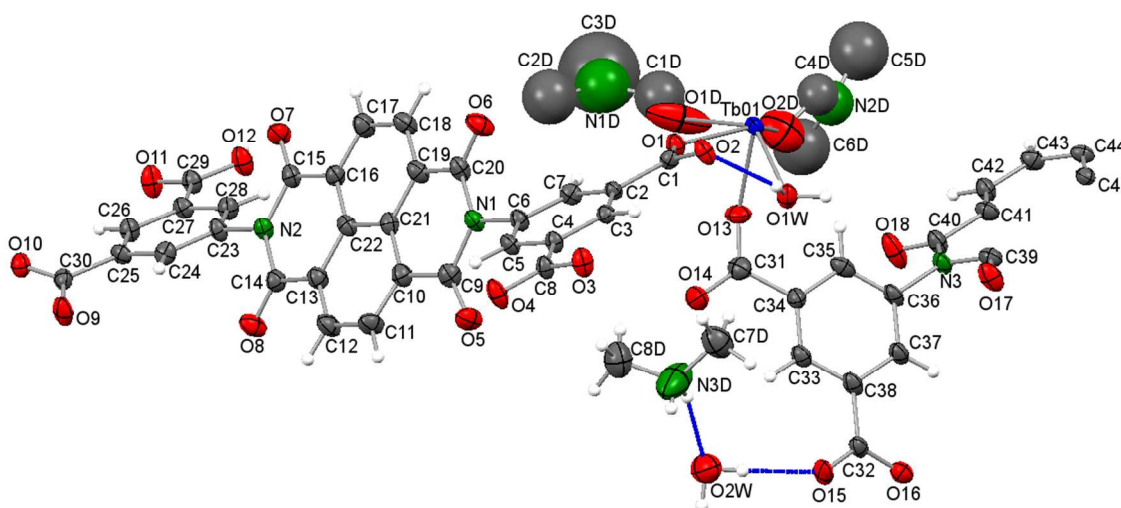


Figure S6. ORTEP representation of the asymmetric unit of MOF-592 displayed with 50% probability. Atom colors: Tb, blue; N, green; O, red; H, white; and C, grey.

Section S4: Topological Analysis

The topologies of MOF-590, -591, and -592 are evaluated by using the *ToposPro* ver 5.3 software program.^{S4}

Table S1. Structural information of MOF-590, -591, and -592.

Compound	Space Group	Topology	Net	Point Symbol	
MOF-590	<i>P</i> -1	nkp	3,3,3,4,4-c; 5-nodal	$\{4.10^2\}_2\{4.6.8^4\}_2\{4.6^2\}_2\{4^2.6^2.8^2\}\{6^2.8\}_2$	
MOF-591				-	$\{4.6^2\}_2\{4^2.6^{12}.8^{14}\}\{6^2.8\}_4$
MOF-592					

It is noted that the new topology discovered for MOF-590 is now included in the Reticular Chemistry Structure Resource Database (rcsr.net/nets/nkp, nkp stands for Nguyen K. Phuong).

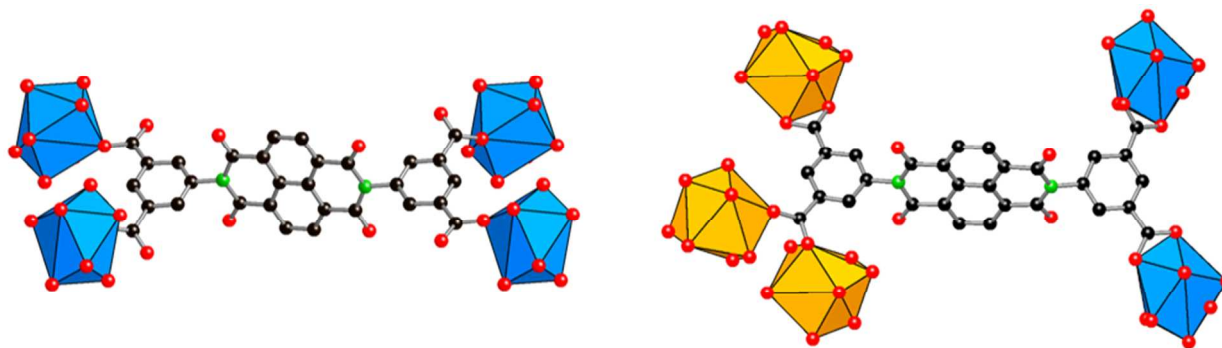


Figure S7. The different connections of BIPA-TC ligand link modes in MOF-590. Atom colors: Nd, blue and orange polyhedra; O, red; C, black; N, green. All H atoms are omitted for clarity.

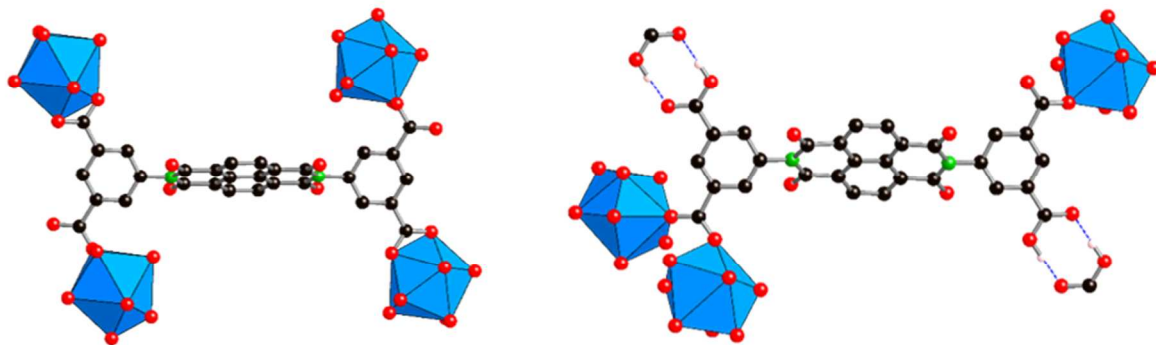


Figure S8. The different connections of BIPA-TC ligand link modes in MOF-592. Atom colors: Tb, blue polyhedra; O, red; C, black; N, green; H of protonated -COOH group, pink spheres. All H atoms, except for those participating in hydrogen bonding, are omitted for clarity.

Section S5: Characterization of MOF-590, -591 and -592.

Powder X-ray Diffraction (PXRD)

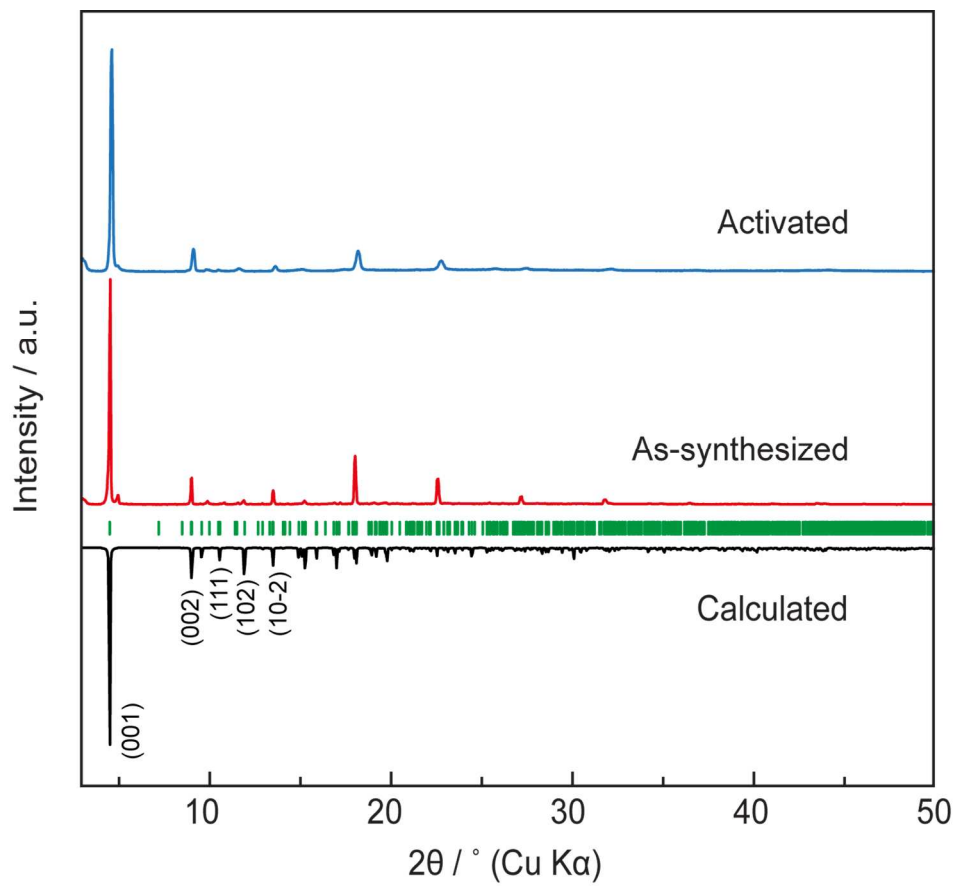


Figure S9. Comparison of the calculated (black) PXRD pattern from the single crystal data with the experimental as-synthesized (red) and activated (blue) PXRD patterns of MOF-590.

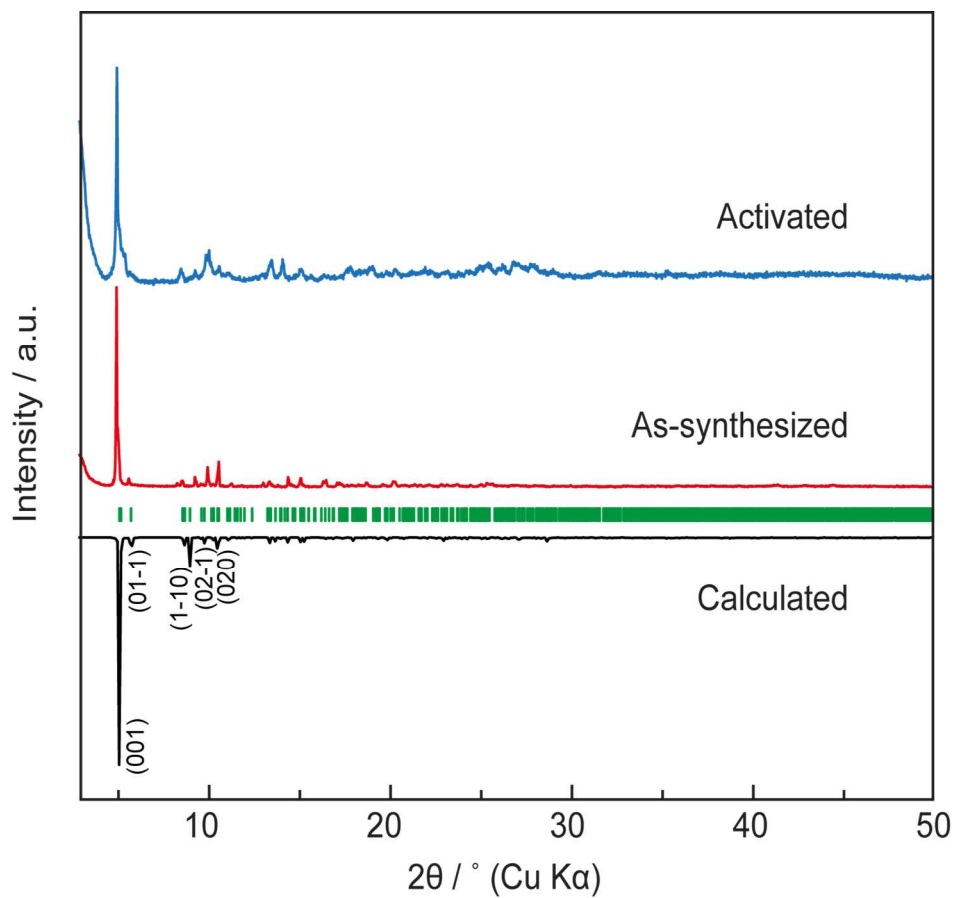


Figure S10. Comparison of the calculated (black) PXRD pattern from the single crystal data with the experimental as-synthesized (red) and activated (blue) PXRD patterns of MOF-591.

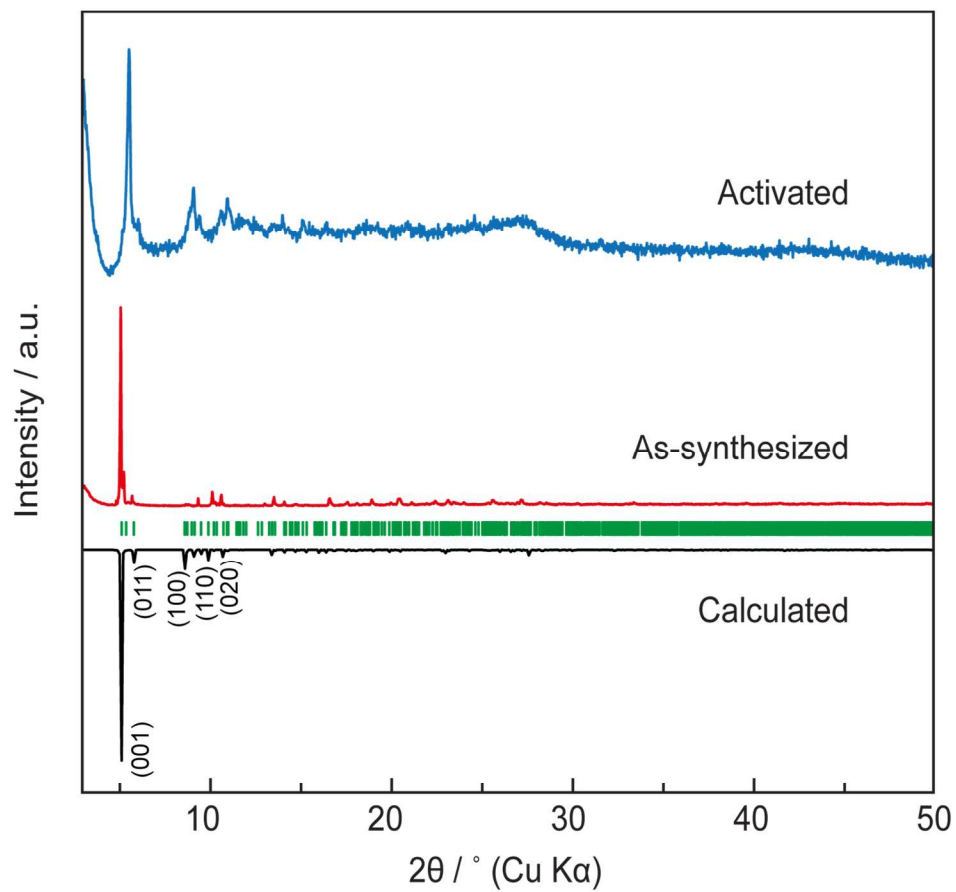


Figure S11. Comparison of the calculated (black) PXRD pattern from the single crystal data with the experimental as-synthesized (red) and activated (blue) PXRD patterns of MOF-592.

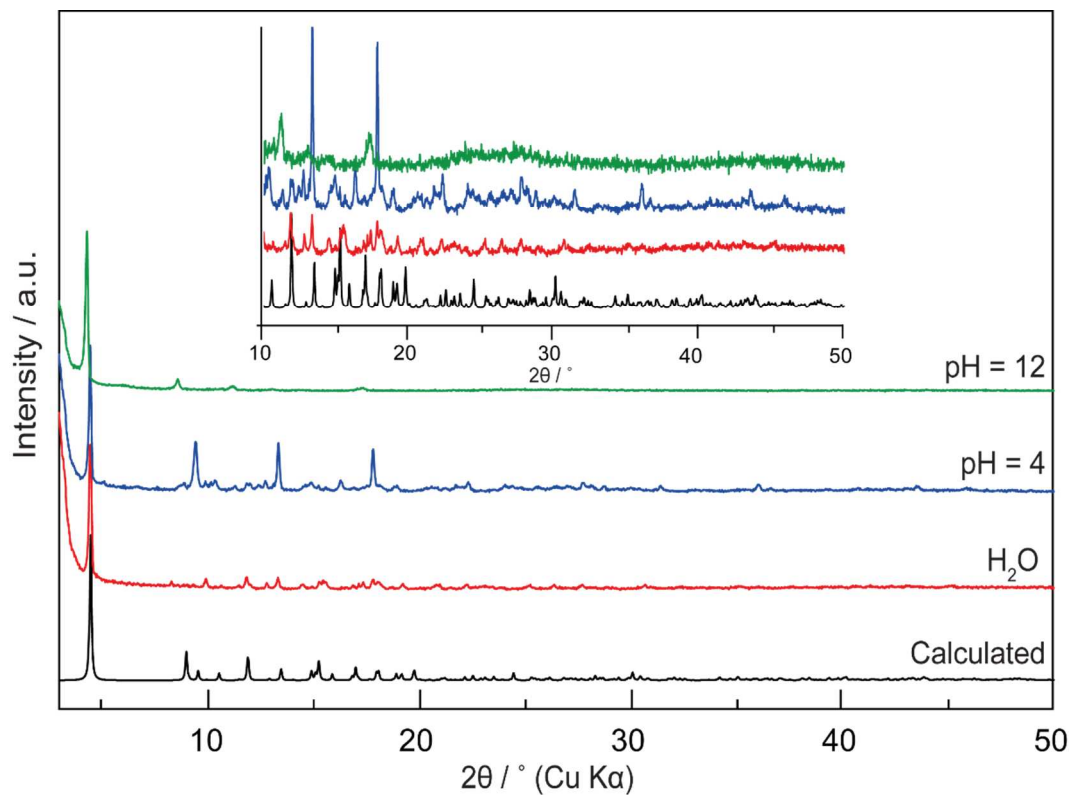


Figure S12. Comparison of the calculated (black) PXRD pattern from the single crystal data with those of MOF-590 after suspension in water (red), acetic acid (pH = 4) (blue), and sodium hydroxide (pH = 12) (green) at room temperature over the course of 7 days. The inset shows magnified view for 2θ range from 10 to 50° .

Thermal Gravimetric Analyses (TGA)

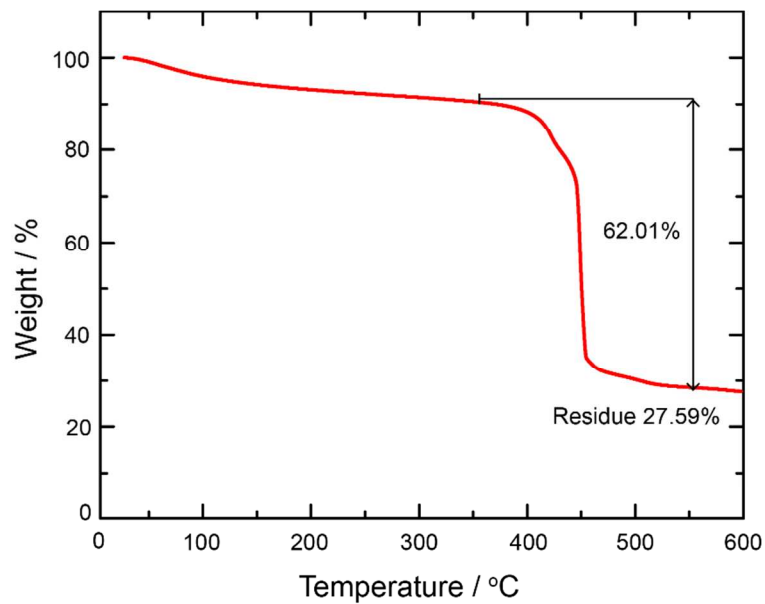


Figure S13. TGA traces of activated MOF-590 at a heating rate of $5\text{ }^{\circ}\text{C min}^{-1}$ under air flow.

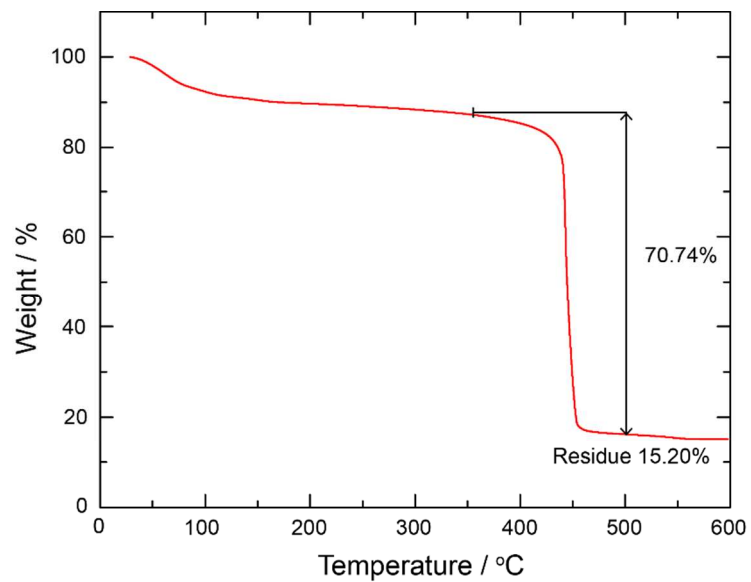


Figure S14. TGA traces of activated MOF-591 at a heating rate of $5\text{ }^{\circ}\text{C min}^{-1}$ under air flow.

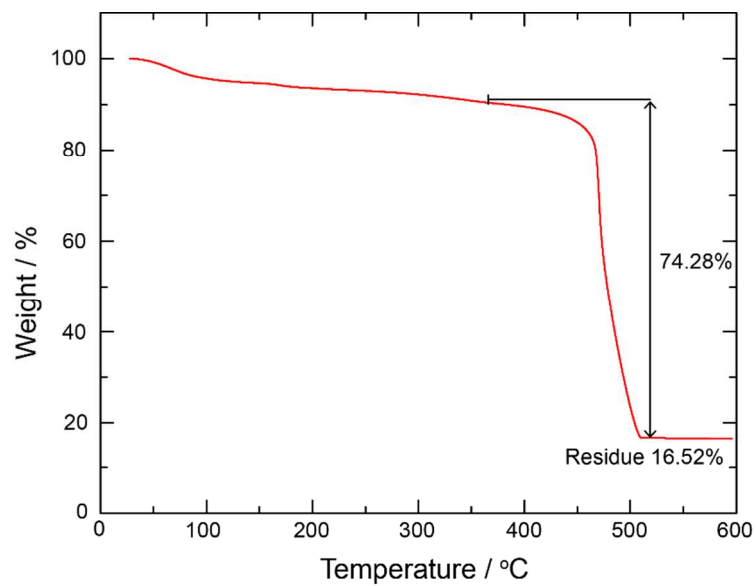


Figure S15. TGA traces of activated MOF-592 at a heating rate of $5\text{ }^{\circ}\text{C min}^{-1}$ under air flow.

Section S6: Gas Adsorption Measurements and Selectivity Calculations

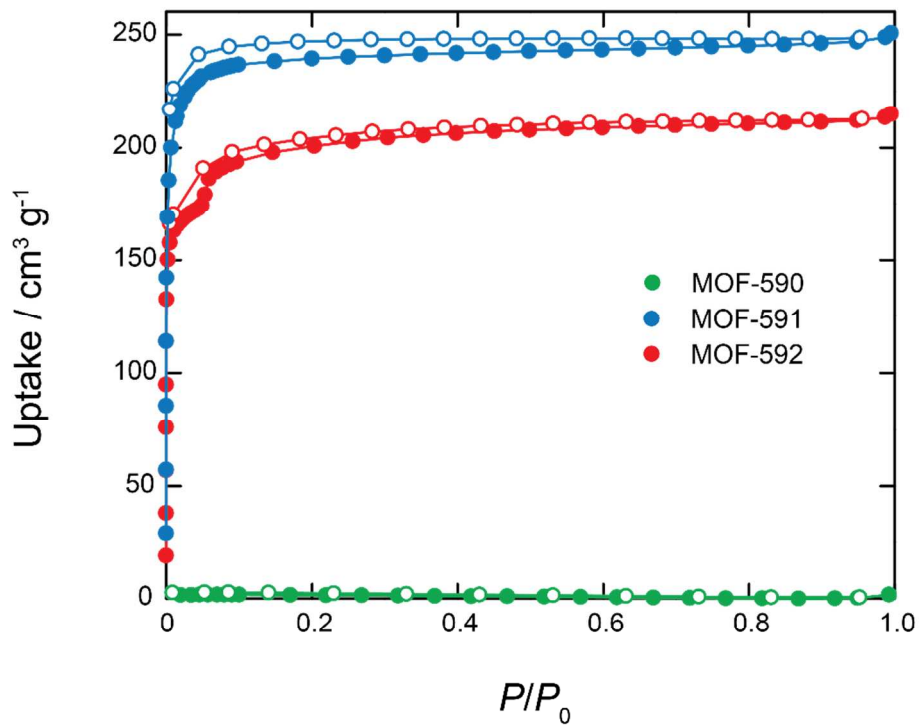


Figure S16. N₂ isotherms of MOF-590 (green), MOF-591 (blue), and MOF-592 (red) at 77 K. Filled and open symbols represent adsorption and desorption branches, respectively. The connecting curves are guides for the eye.

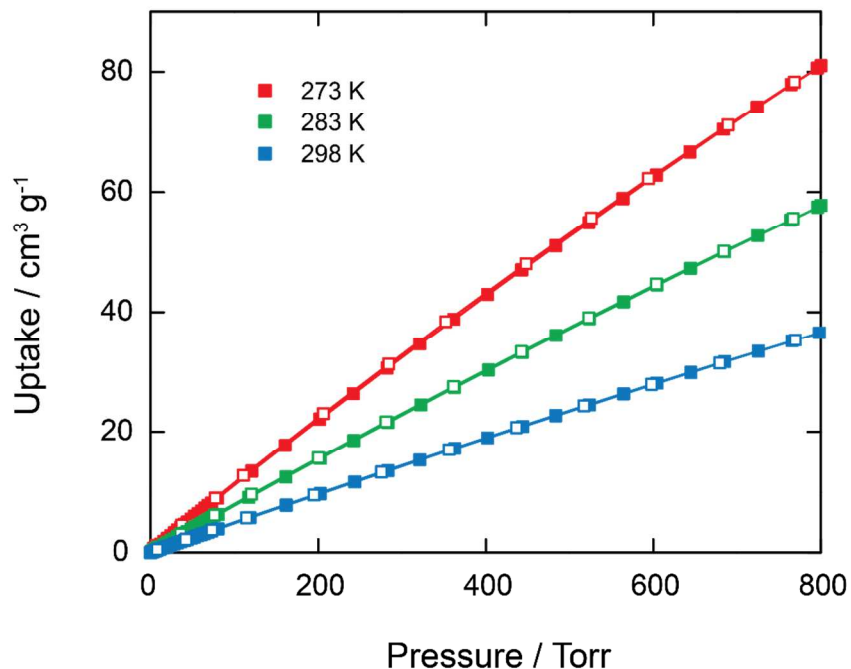


Figure S17. CO₂ isotherms for MOF-591 at 273 (red), 283 (green), and 298 K (blue). Filled and open symbols represent adsorption and desorption branches, respectively. The connecting curves are guides for the eye.

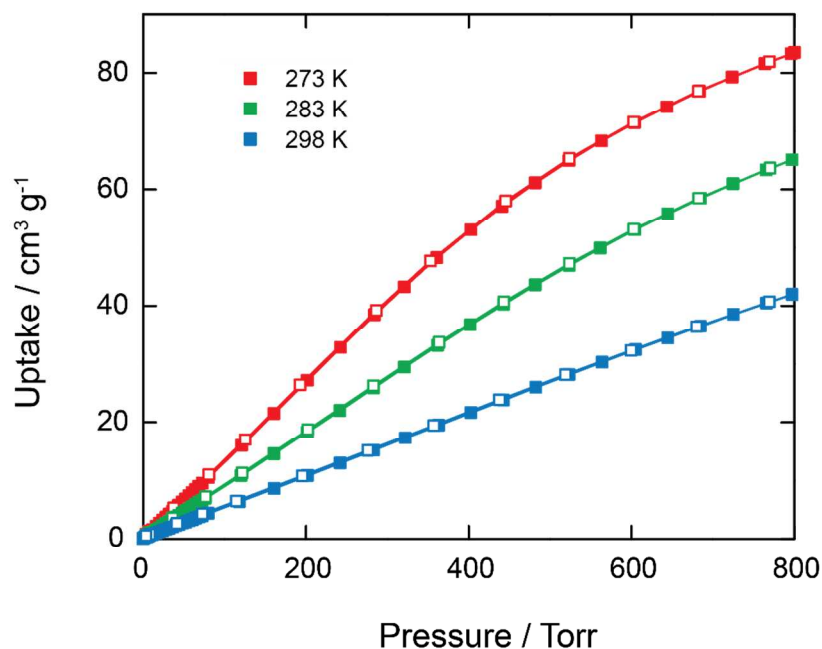


Figure S18. CO₂ isotherms for MOF-592 at 273 (red), 283 (green), and 298 K (blue). Filled and open symbols represent adsorption and desorption branches, respectively. The connecting curves are guides for the eye.

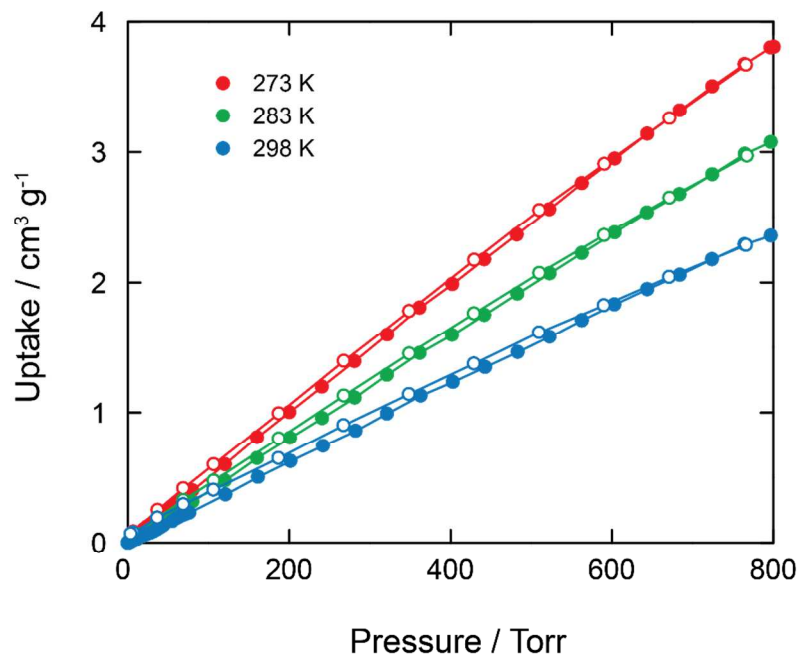


Figure S19. N₂ isotherms for MOF-591 at 273 (red), 283 (green), and 298 K (blue). Filled and open symbols represent adsorption and desorption branches, respectively. The connecting curves are guides for the eye.

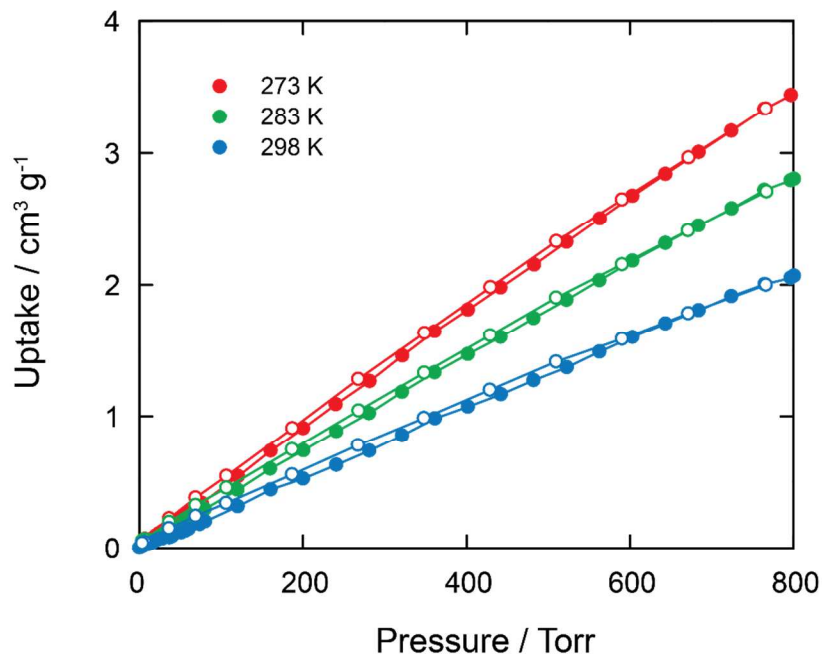


Figure S20. N₂ isotherms for MOF-592 at 273 (red), 283 (green), and 298 K (blue). Filled and open symbols represent adsorption and desorption branches, respectively. The connecting curves are guides for the eye.

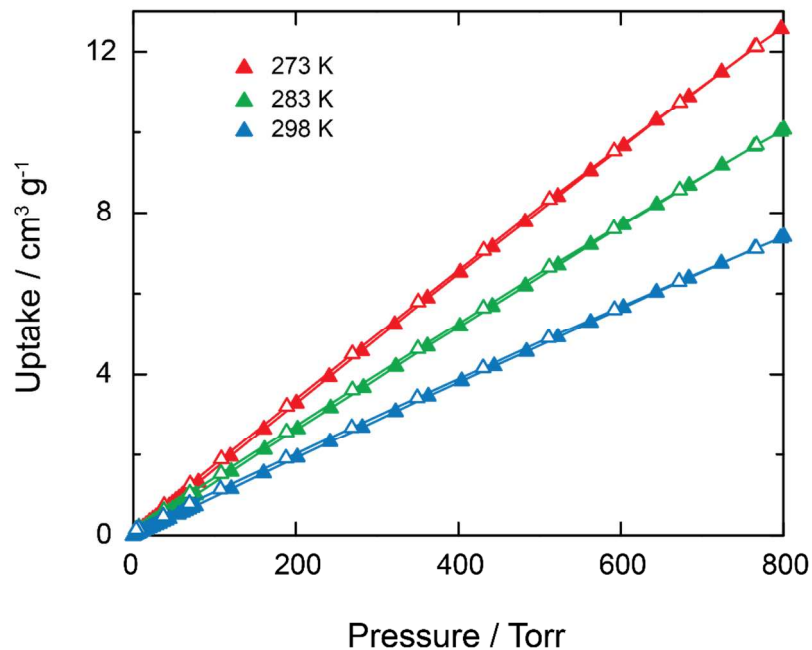


Figure S21. CH₄ isotherms for MOF-591 at 273 (red), 283 (green), and 298 K (blue). Filled and open symbols represent adsorption and desorption branches, respectively. The connecting curves are guides for the eye.

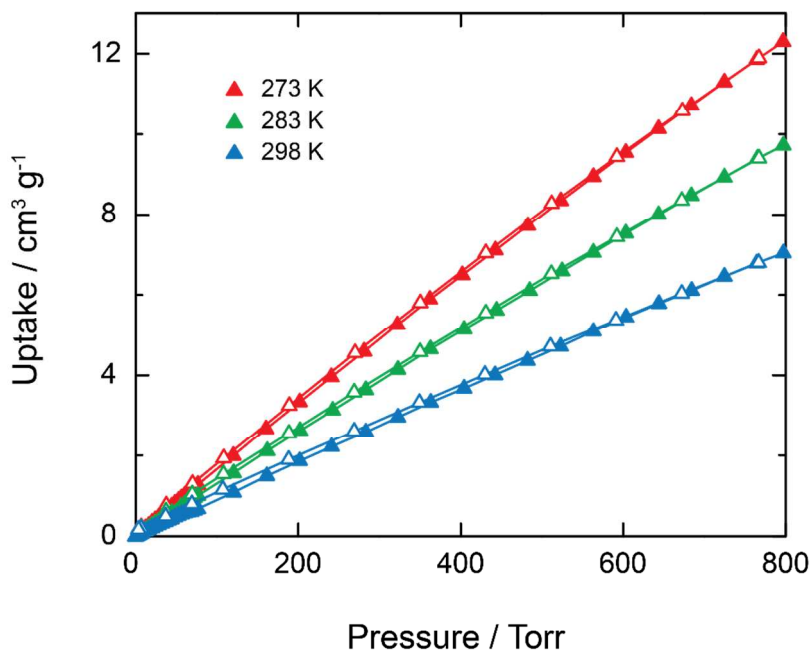


Figure S22. CH₄ isotherms for MOF-592 at 273 (red), 283 (green), and 298 K (blue). Filled and open symbols represent adsorption and desorption branches, respectively. The connecting curves are guides for the eye.

Gas selectivity calculated by Henry's Law

Virial-type equation was employed for estimation of Henry's constant:

$$\ln P = \ln N + \frac{1}{T} \sum_{i=0}^m a_i N^i + \sum_{i=0}^n b_i N^i$$

Where P is pressure, N is the adsorbed amount, T is temperature, a_i and b_i are virial coefficient, and m and n are the number of virial coefficients required for adequate fitting of the isotherms.

As a result, Henry's constant (K_H) at the temperature T can be calculated:

$$K_H = \exp(-b_0) \cdot \exp(-a_0/T)$$

The Henry's Law selectivity for gas component i over j is calculated:

$$S_{ij} = K_{Hi}/K_{Hj}$$

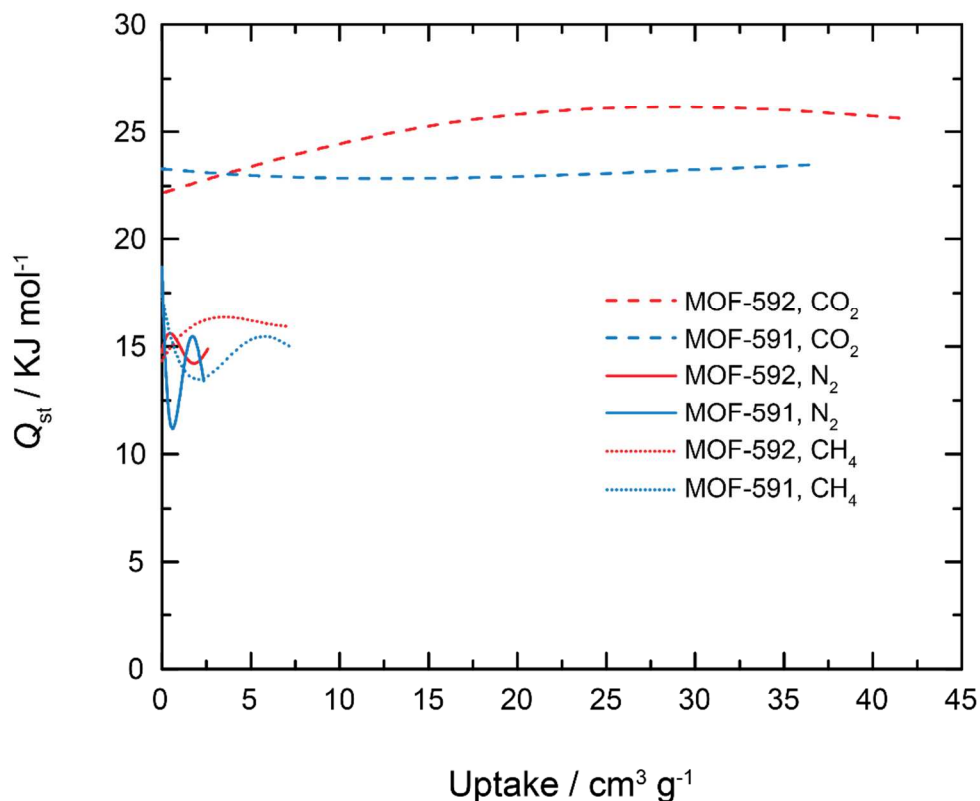


Figure S23. The isosteric heat of adsorption of CO₂ (dashed lines), N₂ (solid lines) and CH₄ (dotted lines) for MOF-591 (blue) and MOF-592 (red).

Section S7: Gas Breakthrough Measurement

Methods

Breakthrough data for MOF-592 was collected using a L&C Science and Technology PSA-300-LC Analyzer. In a typical experiment, activated MOF-890 (0.5142 g) was loaded into a sample bed and a mixture of N₂/CO₂ at 16.8:3.2 (84:16, v/v) sccm, was flowed through the sample bed at room temperature (backpressure = 1.05 bar). The effluent from the bed was monitored by mass spectrometry. The breakthrough time was recorded upon introduction of CO₂ to the bed and was corrected by subtracting the time to breakthrough for a blank sample bed. The material was regenerated, after each cycle, by flowing pure N₂ gas through the MOF-loaded bed.

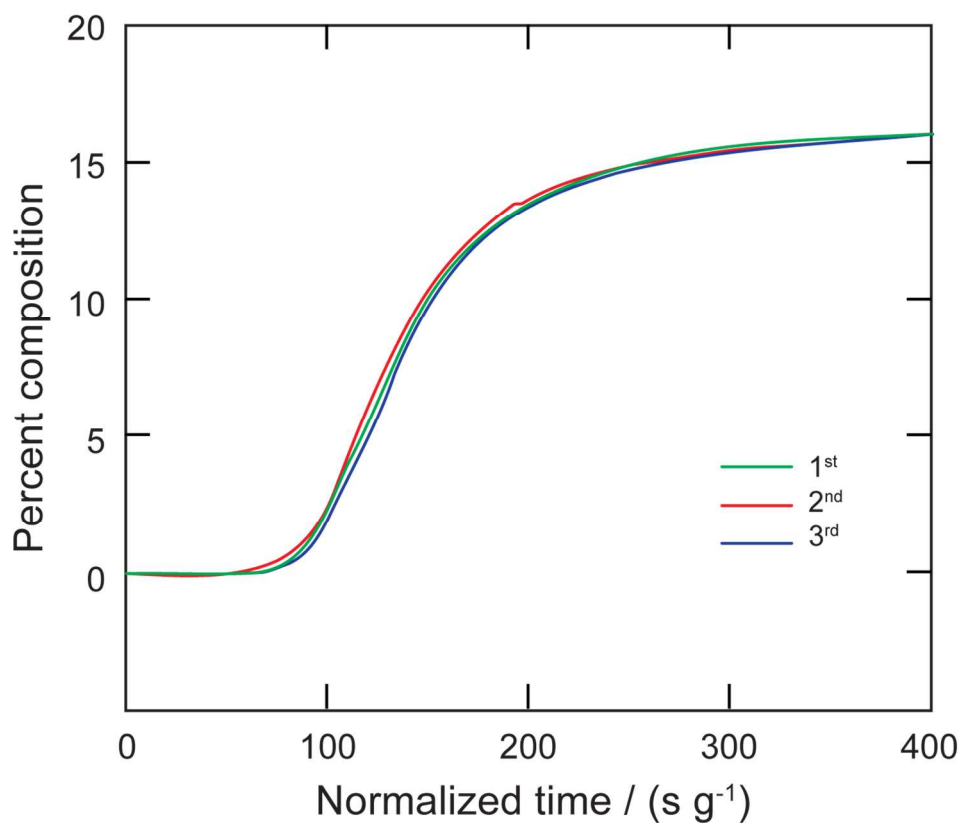


Figure S24. CO₂ breakthrough curves of MOF-592 for CO₂/N₂ (84:16, v/v) separation.

Section S8: Characterization of Materials for Catalysis

PXRD

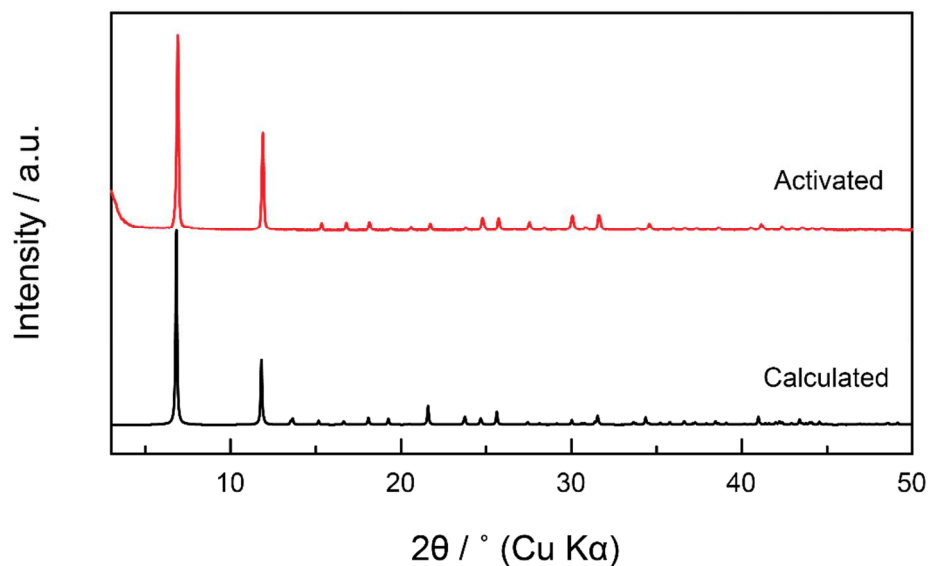


Figure S25. Comparison of the simulated (black) PXRD pattern from the reported structure data with the experimental activated (red) PXRD patterns of Mg-MOF-74.

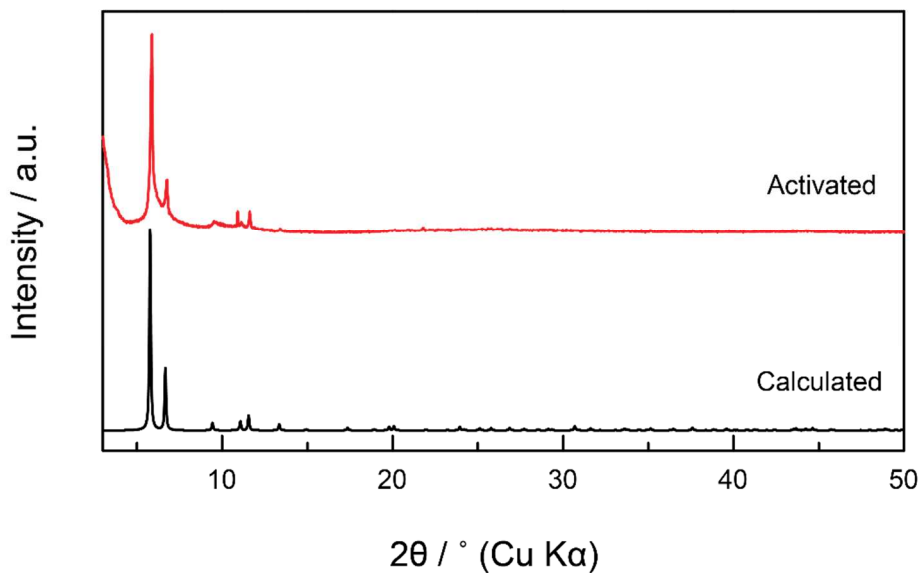


Figure S26. Comparison of the simulated (black) PXRD pattern from the reported crystal structure data with the experimental activated (red) PXRD patterns of UiO-67-bpydc.

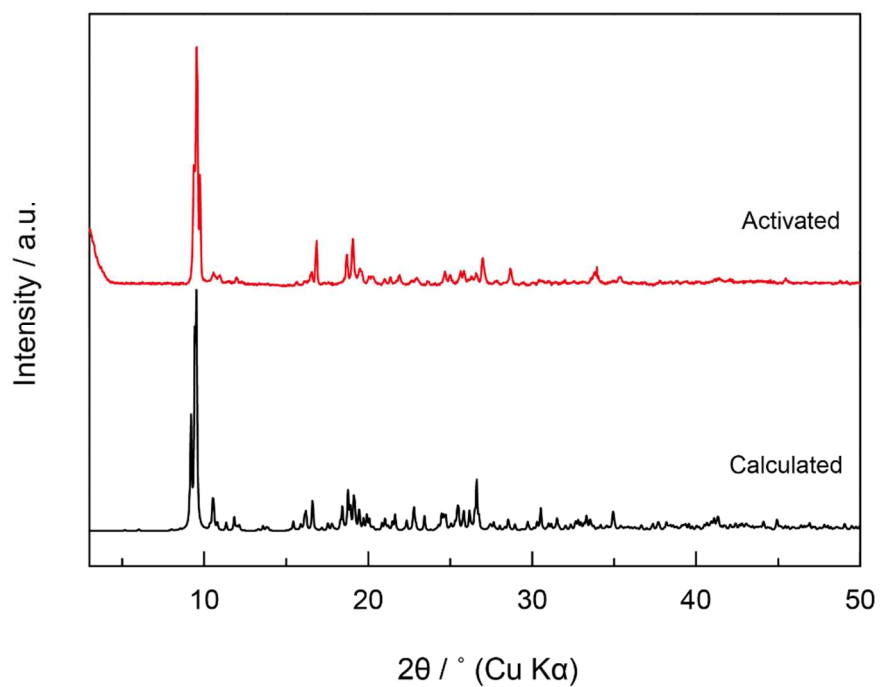


Figure S27. Comparison of the simulated (black) PXRD pattern from the reported crystal structure data with the experimental activated (red) PXRD patterns of Nd-BDC.

Gas Adsorption Measurements

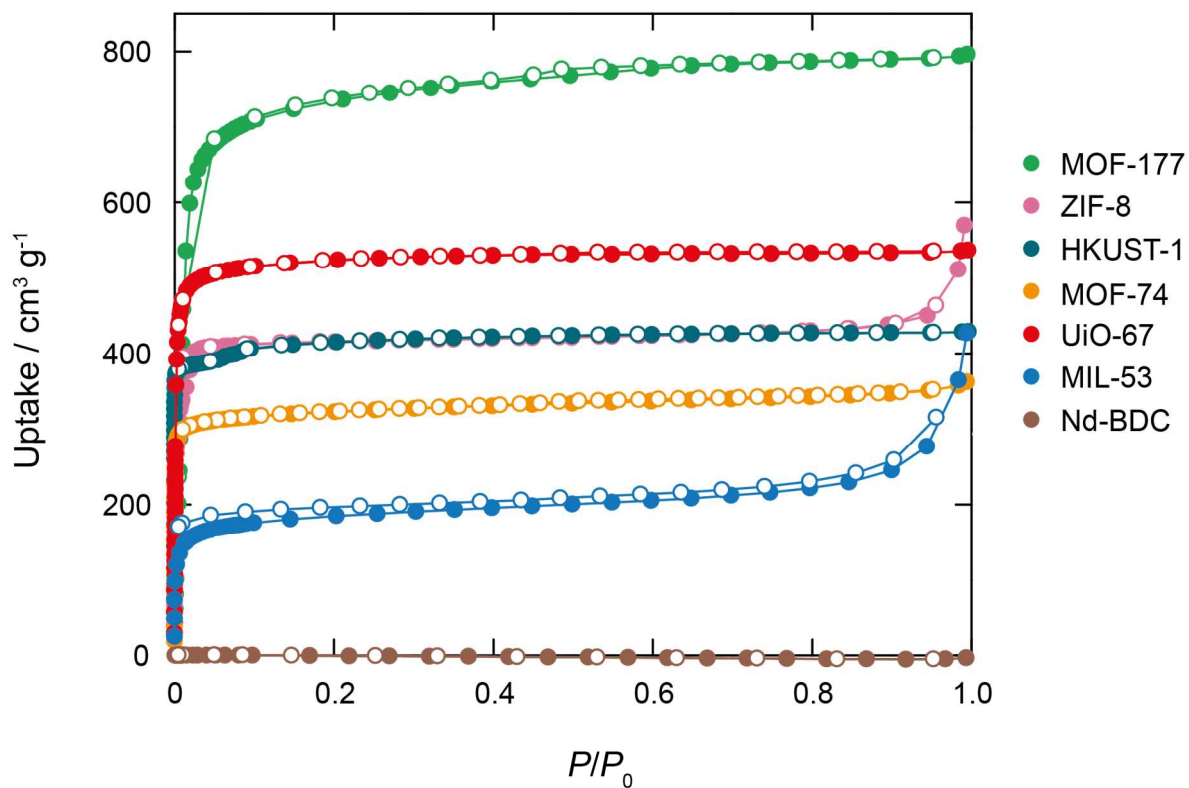


Figure S28. N_2 isotherms of comparative MOFs at 77 K. Filled and open symbols represent adsorption and desorption branches, respectively. The connecting curves are guides for the eye.

FT-IR

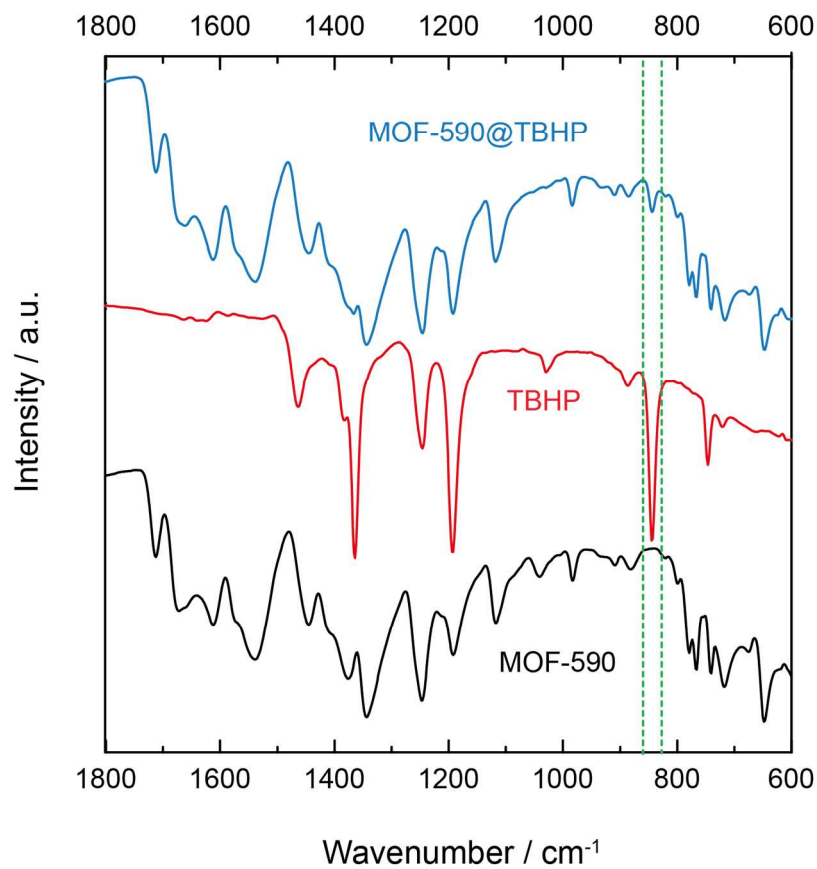


Figure S29. Comparison of FT-IR spectra of activated MOF-590, free *tert*-butyl hydroperoxide (TBHP), and MOF-590@TBHP.

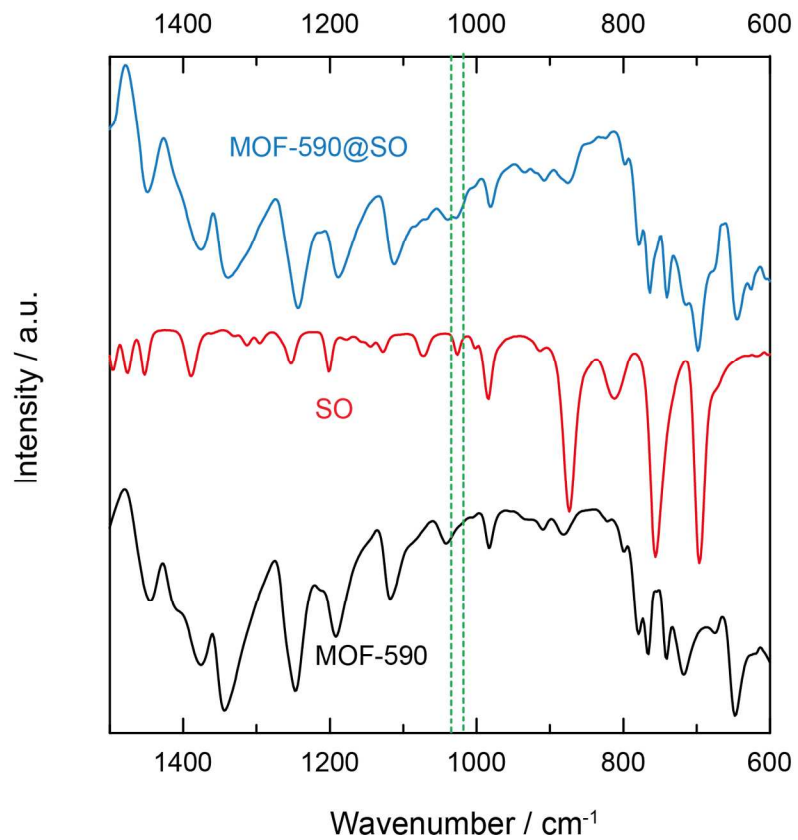


Figure S30. Comparison of FT-IR spectra of activated MOF-590, free styrene oxide (SO), and MOF-590@SO.

Section S9: General Procedure and Studies for the One-pot Oxidative Carboxylation of Styrene and CO₂

After the reaction was completed, the resulting mixture was dissolved in diethyl ether (5 mL) and washed with water (3 × 5 mL). The organic layer was separated, dried over anhydrous sodium sulfate, gravity-filtered and evaporated, under reduced pressure to obtain the styrene carbonate. Yield: 85 %. ¹H NMR (500 MHz, DMSO) δ 7.42–7.48 (m, 5H), 5.85 (t, 1H, *J* = 7.5, 8.0 Hz), 4.87 (t, 1H, *J* = 8.0, 8.5 Hz), 4.40 (t, 1H, *J* = 8.0, 8.5 Hz) ppm. ¹³C NMR (125 MHz, CDCl₃) δ 155.2, 136.8, 129.8, 129.4, 127.1, 78.2, 71.3 ppm. FTIR (KBr, 4000 – 400 cm⁻¹): 2981 (w), 2924 (w), 1778 (s), 1549 (w), 1492 (w), 1456 (w), 1393 (w), 1359 (m), 1328 (w), 1286 (w), 1175 (s), 1058 (s), 958 (w), 903 (w), 830 (w), 757 (s), 696 (s), 609 (w), 554 (w), 490 (w). GC-MS (EI, 70 eV) *m/z*: 164 ([M]⁺), 119, 105, 90.

The overall conversion of styrene was calculated from moles of styrene consumed against the initial moles of styrene used. The yield and selectivity of products were determined from moles of the products formed against the initial moles of styrene used and against the moles of styrene consumed, respectively. S is peak area, n is mole of a substance.

$$\text{Conversion (\%)} = \frac{n_{\text{styrene consumed}}}{n_{\text{styrene initial}}} \times 100\%$$

$$\text{Selectivity (\%)} = \frac{n_{\text{carbonate formed}}}{n_{\text{styrene consumed}}} \times 100\%$$

$$\text{Yield (\%)} = \frac{n_{\text{carbonate formed}}}{n_{\text{styrene initial}}} \times 100\%$$

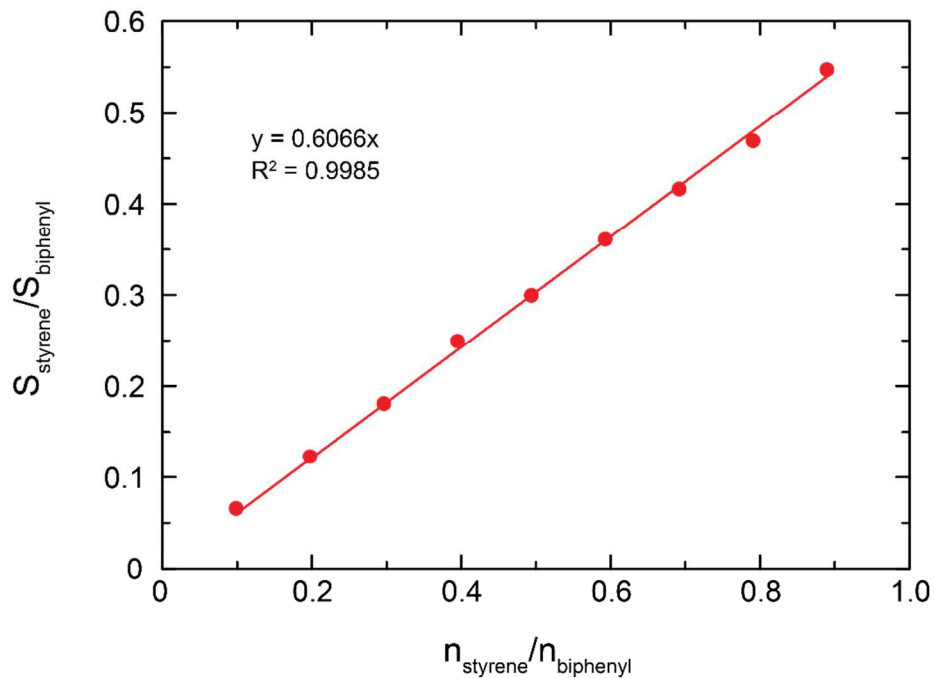


Figure S31. Calibration curve of styrene to determine the conversion, selectivity and GC yield. S is peak area, n is mole of a substance.

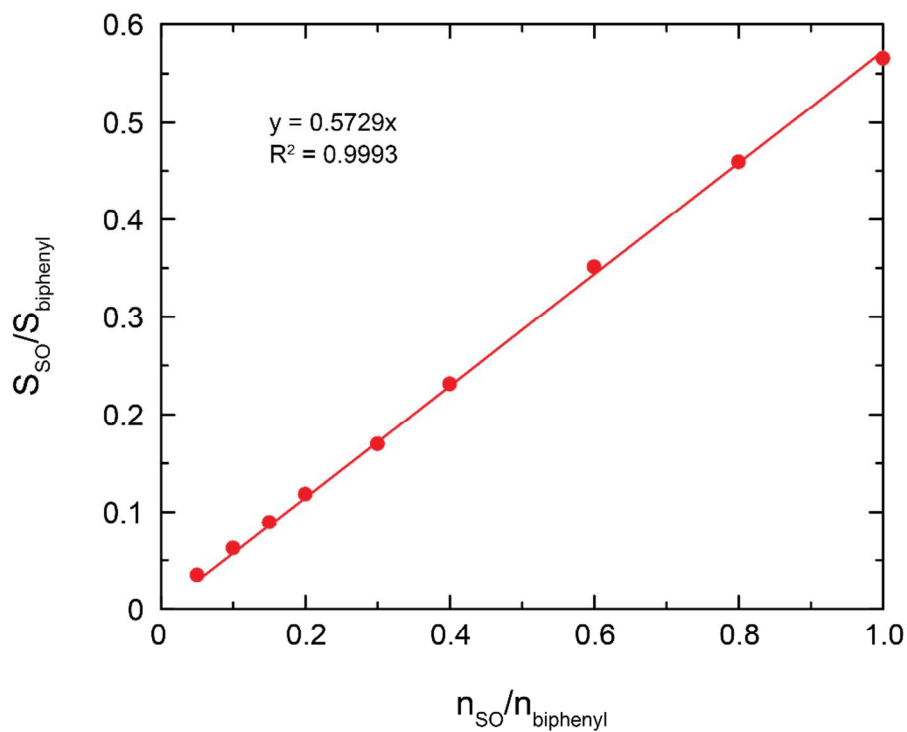


Figure S32. Calibration curve of styrene oxide (SO) to determine the conversion, selectivity and GC yield. S is peak area, n is mole of a substance.

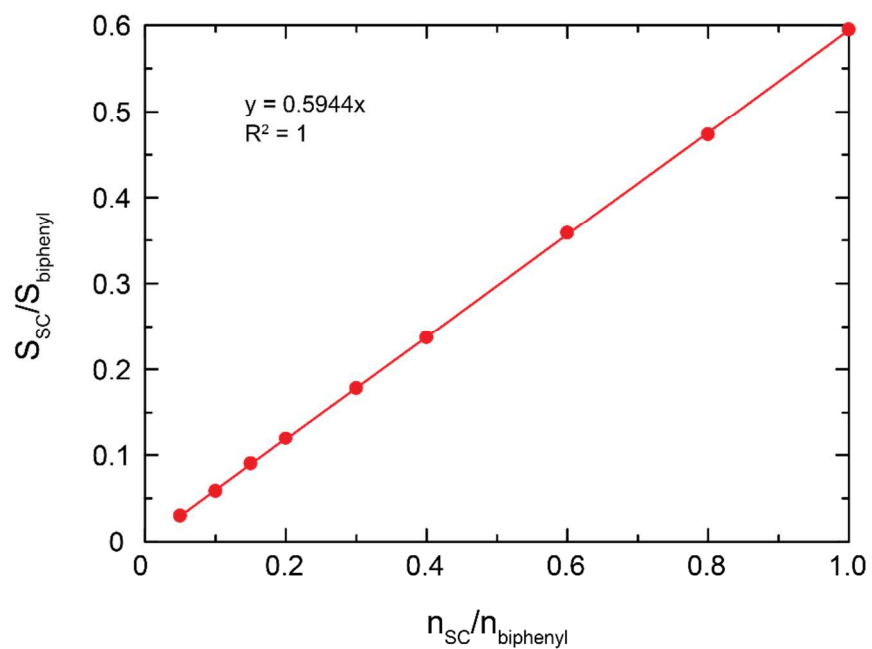


Figure S33. Calibration curve of styrene carbonate (SC) to determine the conversion, selectivity and GC yield. S is peak area, n is mole of a substance.

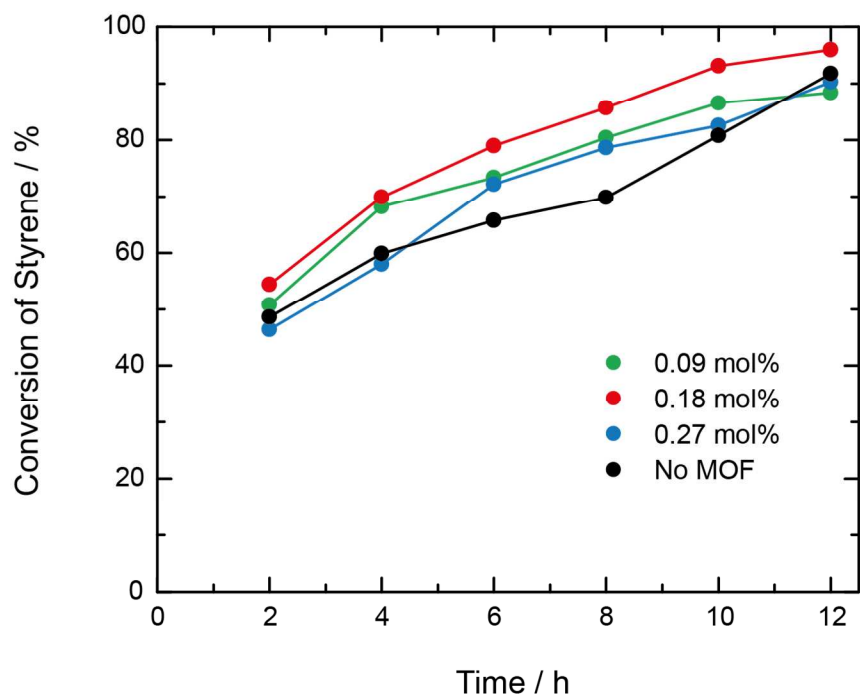


Figure S34. Effect of MOF-590 catalyst amounts on the conversion of styrene in the one-pot oxidative carboxylation.

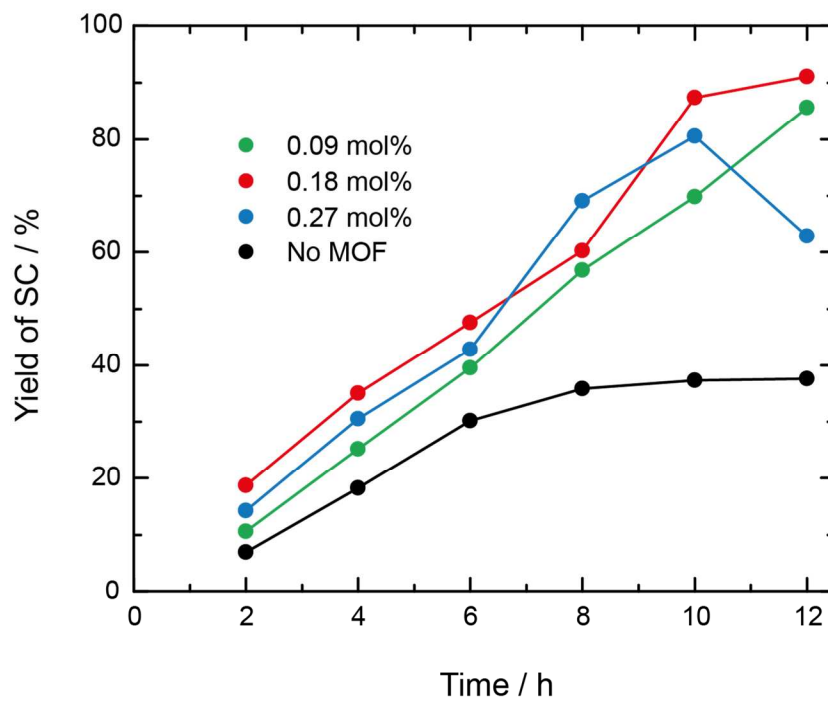


Figure S35. Effect of MOF-590 catalyst amounts on the yield of styrene carbonate (SC) in the one-pot oxidative carboxylation.

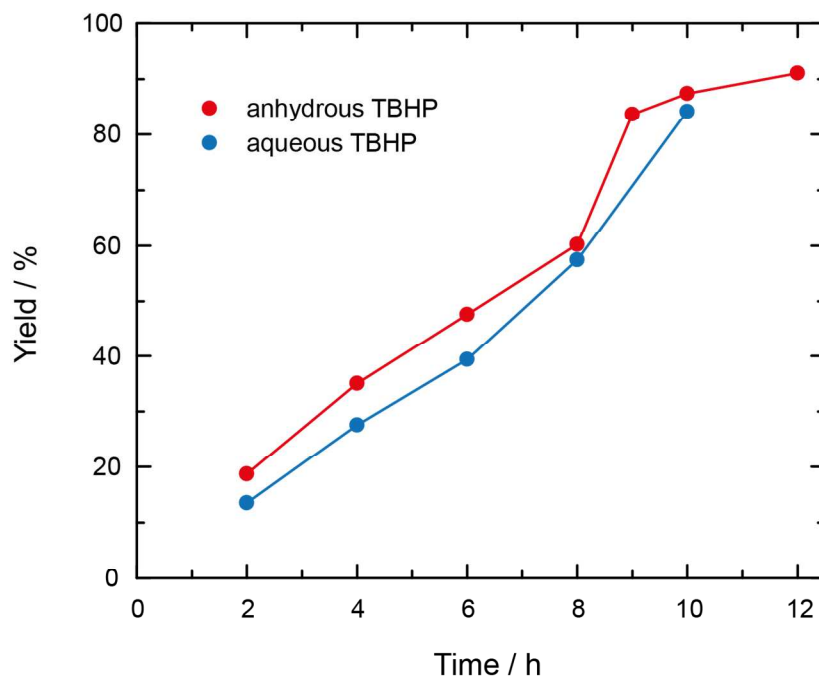


Figure S36. MOF-590 catalyzes the one-pot oxidative carboxylation of styrene and CO₂ with the use of oxidant anhydrous (red), and aqueous (blue) TBHP.

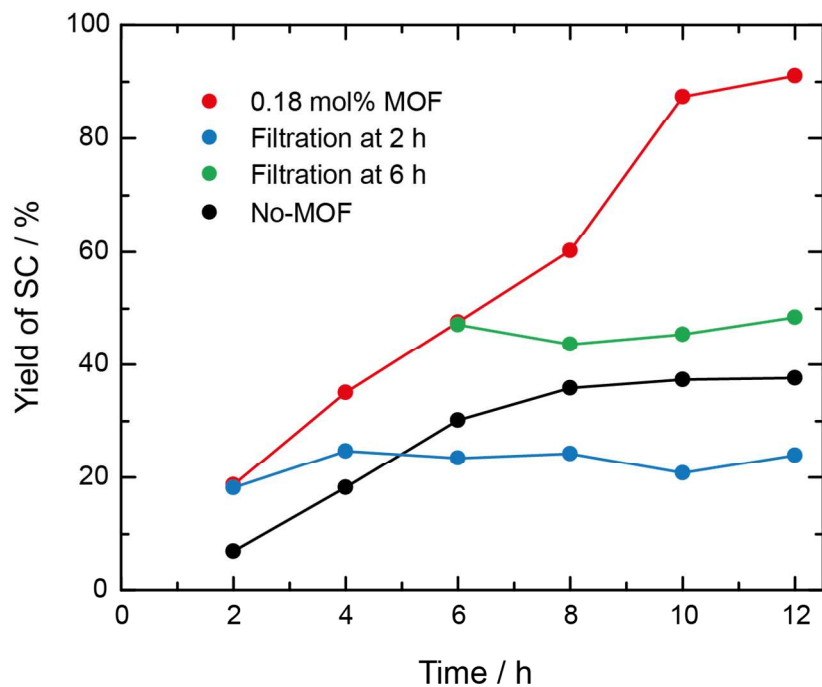


Figure S37. MOF-590 catalyzes the reaction with the model condition (red), catalyst filtration at 2 h (blue), catalyst filtration at 6 h (green), and without MOF catalyst (black).

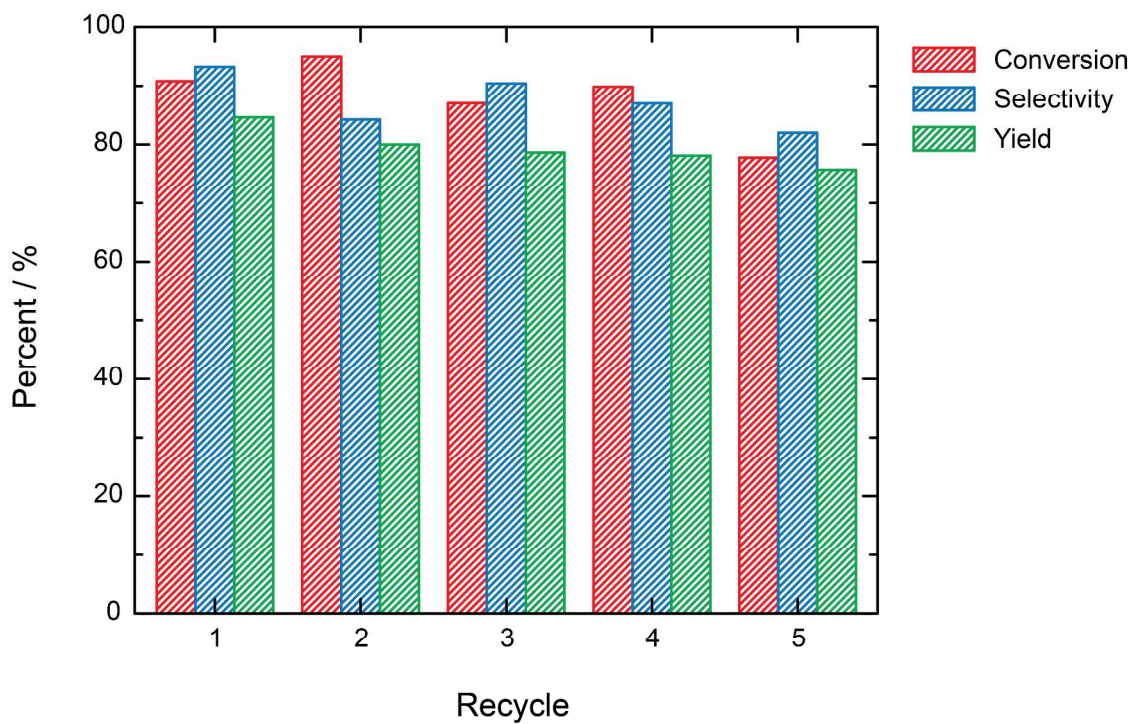


Figure S38. Recycling experiments of MOF-590 for the one-pot oxidative carboxylation.

Section S10: Post-Catalysis Characterization of MOF-590.

Powder X-Ray Diffraction (PXRD)

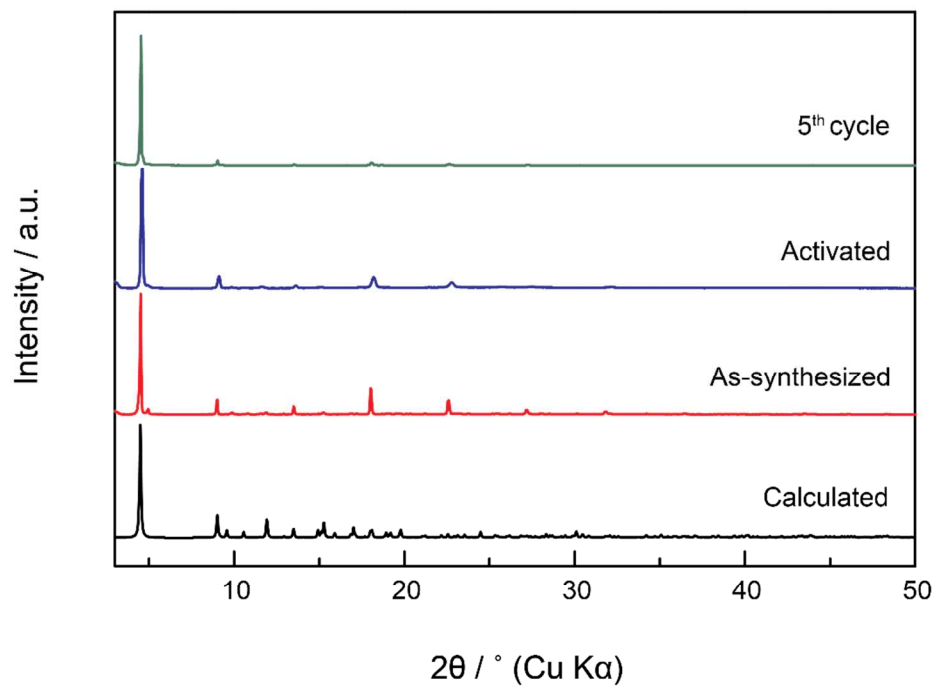


Figure S39. PXRD patterns of calculated MOF-590 from the single crystal data (black), experimental as-synthesized (red), activated (blue), after 5th catalytic reaction (green).

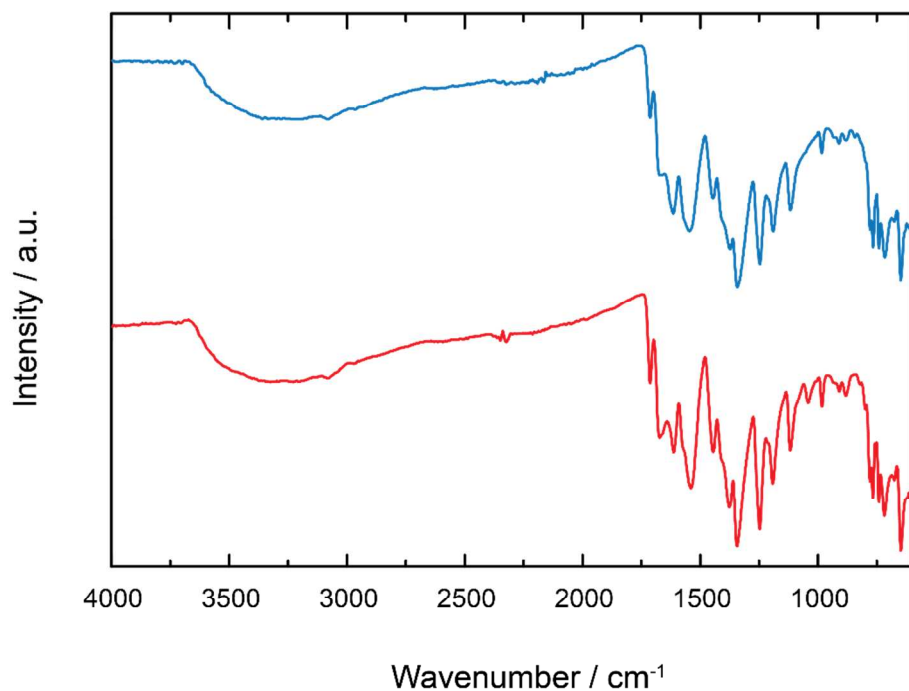


Figure S40. FT-IR of an activated MOF-590 (red) and after 5th time recycling and reusing of MOF-590 (blue).

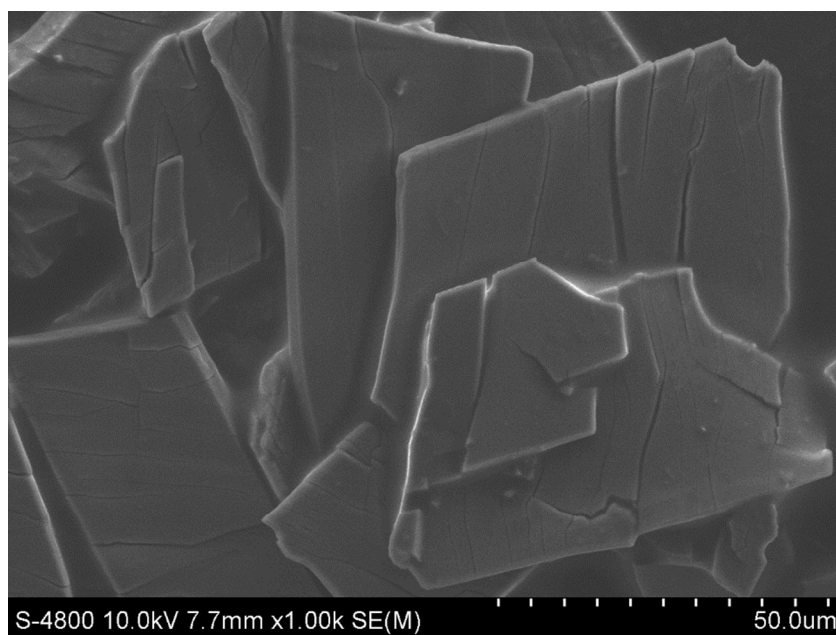
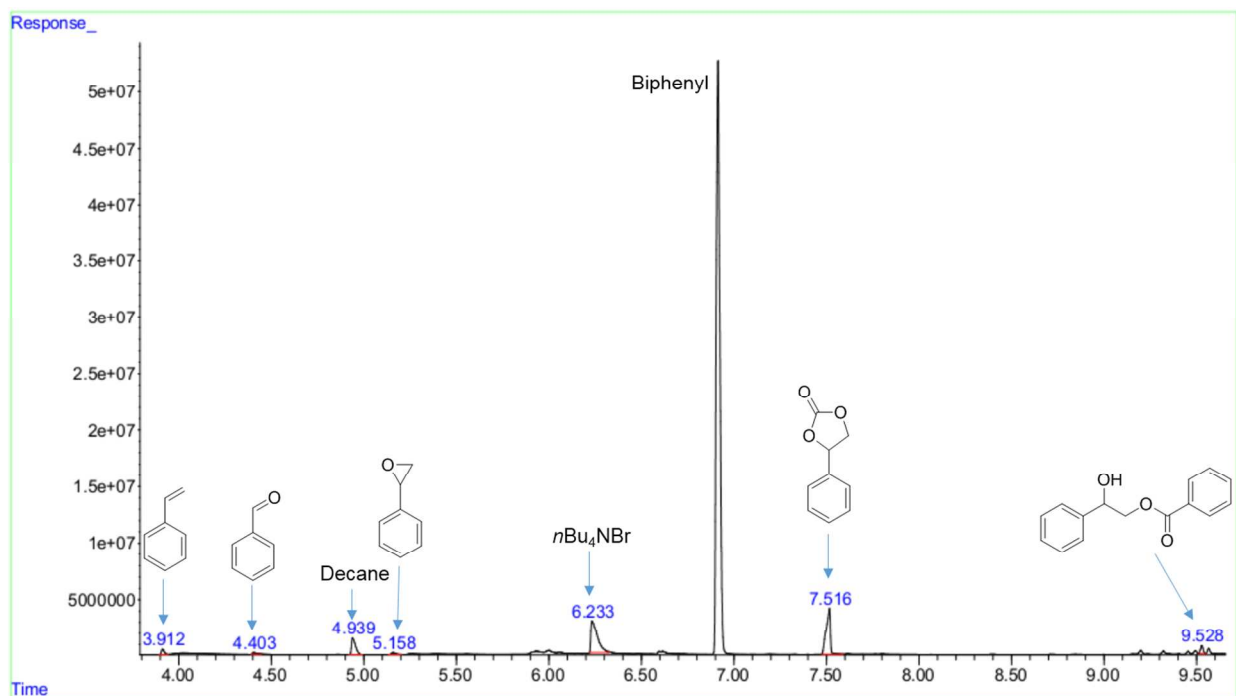


Figure S41. SEM images of the MOF-590 catalyst after catalytic reactions.

Section S11: Mechanism Study for One-pot Oxidative Carboxylation of Styrene and CO₂



Peak #	R.T/ min	Peak height	Peak area	% of total
1	3.912	494198	521610	0.576
2	4.403	157765	262945	0.290
3	4.939	1486418	2174422	2.402
4	5.158	180140	265330	0.293
5	6.233	2877179	7150145	7.898
6	6.914	52631908	72215232	79.764
7	7.516	4106435	6339091	7.002
8	9.528	715850	685305	0.757
Sum of corrected areas: 90536107				

Figure S42. GC chart of the reaction mixture catalyzed by MOF-590.

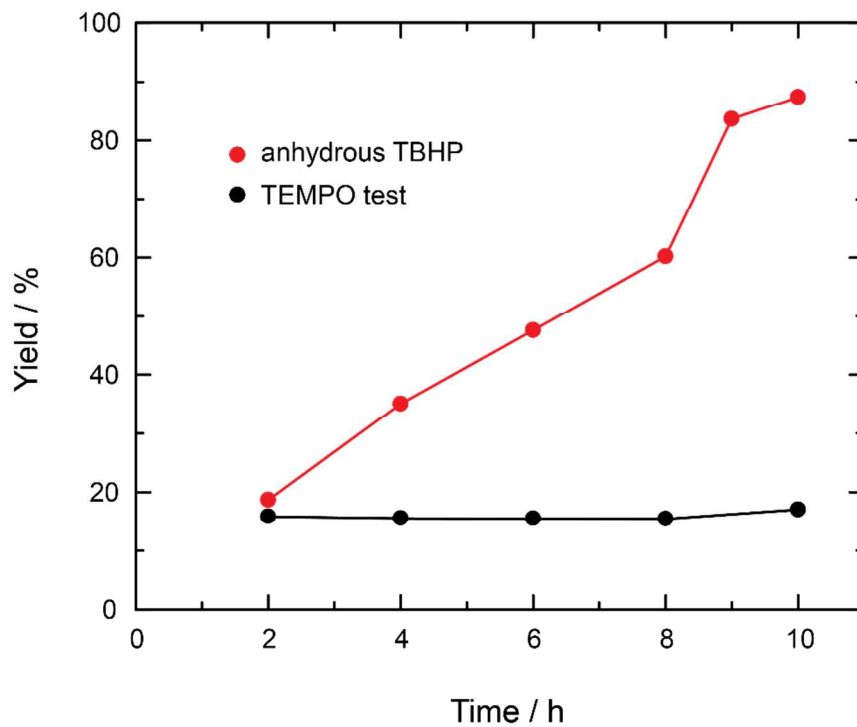


Figure S43. TEMPO test indicates the oxidative carboxylation could not proceed in the presence of radical trapping reagent.

Section S12: References

- [S1] Nguyen, P. T. K.; Nguyen, H. T. D.; Nguyen, H. N.; Trickett, C. A.; Ton, Q. T.; Gutiérrez-Puebla, E.; Monge, M. A.; Cordova, K. E.; Gándara, F. New Metal–Organic Frameworks for Chemical Fixation of CO₂. *ACS Appl. Mater. Interfaces* **2018**, *10*, 733-744.
- [S2] Decadt, R.; Van Hecke, K.; Depla, D.; Leus, K.; Weinberger, D.; Van Driessche, I.; Van Der Voort, P.; Van Deun, R. *Inorg. Chem.* **2012**, *51*, 11623-11634.
- [S3] Cairns, A. J.; Perman, J. A.; Wojtas, L.; Kravtsov, V. C.; Alkordi, M. H.; Eddaoudi, M.; Zaworotko, M. J. Supermolecular Building Blocks (Sbbs) and Crystal Design: 12-Connected Open Frameworks Based on a Molecular Cubohemioctahedron. *J. Am. Chem. Soc.* **2008**, *130*, 1560-1561.
- [S4] Blatov, V. A.; Shevchenko, A. P.; Proserpio, D. M. Applied Topological Analysis of Crystal Structures with the Program Package Topospro. *Cryst. Growth Des.* **2014**, *14*, 3576-3586.